



Stress redistribution and fracture propagation during restimulation of gas shale reservoirs



Xiang Li^{a,*}, Jiehao Wang^{a,b}, Derek Elsworth^a

^a John and Willie Leone Family Department of Energy and Mineral Engineering, EMS Energy Institute and G3 Center, Pennsylvania State University, University Park, PA 16802, USA

^b State Key Laboratory of Geomechanics and Deep Underground Engineering, China University of Mining and Technology, Xuzhou, Jiangsu 221008, China

ARTICLE INFO

Keywords:

Hydraulic fracturing
Refrac
Stress redistribution
Stress reversal region
Fracture propagation

ABSTRACT

Restimulation of previously hydraulically-fractured wells can restore productivity to near original levels. Understanding the stress state resulting from the original hydraulic fracturing and subsequent depletion is vital for a successful refracturing treatment. The stress obliquity in the vicinity of the wellbore, due to production from a previously introduced hydraulic fracture, promotes a new concept – that of altered-stress refracturing which allows fractures to propagate into previously unstimulated or understimulated areas and therefore enhancing recovery. In this study, a coupled poromechanical model is used to define stress redistribution and to define optimal refrac timing as defined by maximizing the size of the stress reversal region. Key factors include the time dependency of the stress reorientation, the threshold stress ratio $\sigma_{h\ max}/\sigma_{h\ min}$ and the influences of permeability anisotropy/heterogeneity, pressure drawdown and rock-fluid properties. The results show that stress reorientation develops immediately as the reservoir begins to produce. This stress reversal region extends to a maximum extent before retreating as the direction of the maximum principal stress gradually returns to the initial state. The optimal refrac timing and the size of the stress reversal region are positively correlated with pressure drawdown and Biot coefficient, negatively correlated with stress ratio $\sigma_{h\ max}/\sigma_{h\ min}$ ratio and Poisson's ratio and ambiguously correlated with permeability anisotropy. Permeability magnitude and porosity have no influence on the size of the resulting zone but are negatively and positively correlated to the timing, respectively. Permeability heterogeneity has no influence on the size nor the timing. Coupled fluid flow and damage-mechanics simulations follow fracture propagation under the effect of stress redistribution during refracturing treatments. These results define the evolving path of secondary refracture as it extends perpendicular to the initial hydrofracture and ultimately turns parallel to the hydrofracture as it extends beyond the stress-reversal region. This discrete model confirms the broader findings of the continuum model.

1. Introduction

After hydraulic fracturing, hydrocarbon production results in a decrease in pore pressure, which in turn results in anisotropic changes in the stress field in the vicinity of the wellbore. Mack and Elbel (Mack and Elbel, 1994; Elbel and Mack, 1993) first demonstrated that production from a fractured well results in the stresses surrounding the fracture decreasing over time as the reservoir depletes. This decrease is greater in the direction parallel to the fracture than normal to the fracture. This work was extended by Siebrits (Siebrits et al., 2000) who introduced the concept of a stress reversal region (Fig. 1) and investigating the evolution of the stress redistribution around a producing fracture using a 3D numerical simulator to examine the dimensions of the stress reversal region as a function of various

reservoir properties. In a tight gas reservoir, the stress redistribution allows refracturing to propagate into the undepleted or less depleted region where elevated pore pressures have not been significantly depleted - allowing production to significantly increase. Production-induced stress reorientation has been monitored using seismic methods (Sayers, 2004) and reorientation of hydraulic fractures as a result of stress redistribution has already been confirmed by surface tiltmeter measurements in the Barnett Shale (Weng and Siebrits, 2007; Wolhart, 2001), the Daqing oilfield (Liu et al., 2008) and the Codell formation of the Wattenberg field in Colorado (Wolhart et al., 2007). Field tests conducted to verify refracturing reorientation in the Barnett Shale show a significant increase in production (Siebrits et al., 2000). Lab-scale tests have also demonstrated that a fracture can reorient itself as the stress field changes (Liu et al., 2008).

* Corresponding author.

E-mail address: xzl111@psu.edu (X. Li).

<http://dx.doi.org/10.1016/j.petrol.2017.04.027>

Received 9 May 2016; Received in revised form 19 April 2017; Accepted 20 April 2017

Available online 21 April 2017

0920-4105/ © 2017 Elsevier B.V. All rights reserved.

Nomenclature

Notation definition

σ [MPa]	Cauchy stress tensor
ε	Strain tensor
C [MPa]	Elasticity matrix
α_B	Biot-Willis coefficient
p_f [MPa]	Fluid pore pressure
I	Unit matrix
ζ [kg]	Increments in fluid content
ε_{vol}	Volumetric strain
M [MPa]	Biot modulus
S	Storage coefficient
v [m/s]	Darcy velocity
∇p [MPa/m]	Pore pressure gradient
T [s]	Time
Q_m [kg]	Source of mass
ρ_{av} [kg/m ³]	Average density of fluid and solid matrix
g [m/s ²]	Gravitational acceleration
u [m/s]	Flow velocity
τ	Dimensionless time
L_f [m]	Fracture half-length
σ_1 [MPa]	Maximum principal stress
σ_3 [MPa]	Minimum principal stress
f_{t0} [MPa]	Uniaxial tensile strength

f_{c0} [MPa]	Compressive strength
θ [°]	Internal friction angle
P [MPa]	Pore pressure
E_0 [MPa]	Elasticity modulus of an REV before the initiation of damage
E [MPa]	Elasticity modulus of an REV after the initiation of damage
D	Damage variable
ε_{t0}	Maximum tensile strain
ε_{c0}	Compressive principal strain
k_0 [m ²]	Initial permeability
α_k	Damage-permeability coefficient
k [m ²]	Permeability
μ [Pa·s]	Viscosity
E [Pa]	Young's modulus
ρ_s [kg/m ³]	Rock density
ρ_f [kg/m ³]	Fluid density
ν	Poisson's ratio
α	Biot coefficient
ϕ	Porosity
c_f [1/Pa]	Fluid compressibility
p_{res} [MPa]	Initial reservoir pressure
p_{wf} [MPa]	Bottomhole flowing pressure
σ_{max} [MPa]	Maximum principal stress
σ_{min} [MPa]	Minimum principal stress
w [mm]	Fracture maximum width

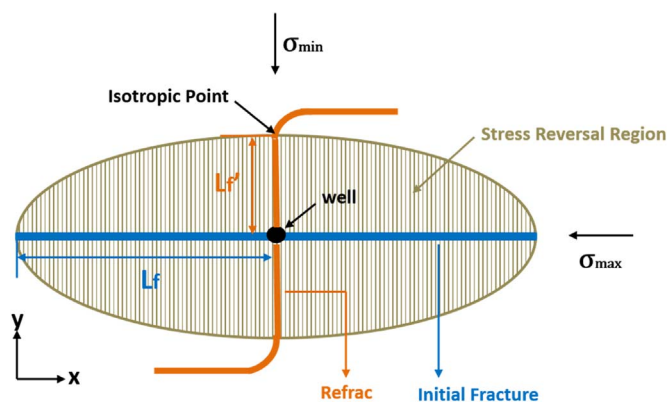


Fig. 1. Stress reversal region concept (Siebrits and Elbel, 1998).

The concept of a stress reversal region (also known as: stress reorientation, stress obliquity or stress redistribution) is illustrated in Fig. 1. The stress reversal region relies on an initially small difference between the maximum and minimum horizontal stresses – this is often true for tight gas reservoirs (Aghighi et al., 2009). The direction of the maximum horizontal stress is aligned parallel to the initial fracture. During the depletion of the reservoir, the stresses reorient due to the change in pore pressure (Biot, 1955). During production, the reservoir will first experience linear flow towards the fracture with this later switching to radial flow (Fig. 1). The stress reduction will be higher in the direction parallel to the initial fracture (Siebrits and Elbel, 1998). Therefore it is possible that the initial small stress difference can be overcome. As a result, a stress reversal region will develop around the fracture as shown (grey ellipse) in Fig. 1 and a secondary fracture may propagate orthogonal to the initial fracture. As production continues the stress reversal region expands (Elbel and Mack, 1993). The magnitude of induced stress differences around the fracture first increase and subsequently decrease due to the propagation of a zone of extension/dilation. Therefore the optimal timing for the refracture treatment must be identified to maximize recovery. Refracturing at the

optimal time creates a new fracture which first initiates and then propagates perpendicular to the initial fracture. This potentially penetrates the minimally depleted or undepleted formation. At the isotropic point (Fig. 1), where the stresses in the x- and y-directions are equal, the fracture turns in a direction parallel to the initial fracture. In the following, the size of the stress reversal region is characterized by the parameter L_f which represents the distance from the wellbore to the isotropic point as shown in Fig. 1.

This stress reorientation is dependent on many factors, including stress anisotropy, permeability anisotropy, production rate/pressure drawdown and fracture toughness, among others (Zhai and Sharma, 2007; Singh et al., 2008). Some case studies identify the basic behavior of the reservoir stress field during production or injection as a proxy for refrac reorientation (Chen and Lawrence, 2001; Hagemann et al., 2012), but few consider the coupled poroelastic and mechanical effects (Roussel, 2011) (Hagemann et al., 2012; Zhou et al., 2015). This study examines the optimal refrac-time and the evolution of the dimensions of the stress reversal region under various reservoir conditions by considering the coupled effects of poroelasticity. Key factors include the time dependency of the stress reorientation, threshold of the stress ratio $\sigma_{h\ max}/\sigma_{h\ min}$ for the presence of the stress reversal region, the influences of permeability anisotropy/heterogeneity, pressure drawdown and rock-fluid properties. These processes are examined in the following to illuminate best practices for refracturing. Finally, fracture propagation during the refrac treatment, considering, accommodating stress redistribution, rock damage and fluid flow. This is used to confirm the mode of fracture propagation during the treatment and to confirm results from the continuum analysis defining the conditions when refracturing may be successful.

2. Model development

Stress reversal in the region around a fractured well results from the propagation of the original hydraulic fracture with the pore pressure drawdown effects superposed. In this paper, the coupling between both phenomena is explored to examine the extent and time dependency of the stress reversal region around the fractured produc-

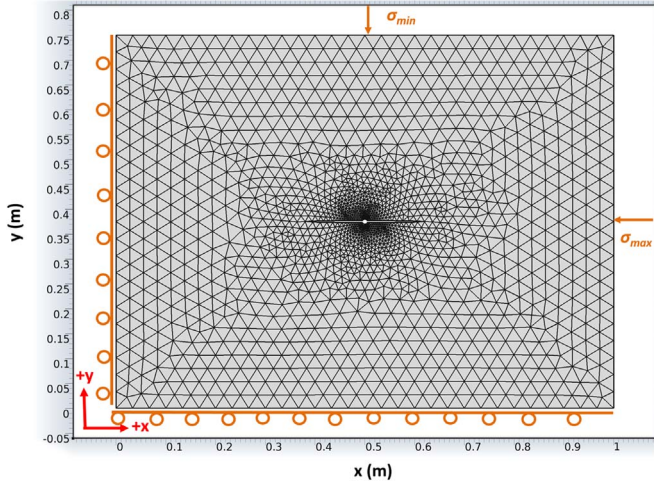


Fig. 2. Reservoir geometry.

tion well under various reservoir conditions.

2.1. Governing equation

The coupled fluid-flow/mechanical behavior in an isothermal linear poroelastic material is governed by the relations between pore pressure p_f , Darcy's velocity v , stress tensor σ , strain tensor ε , and the increment in fluid content ζ (Biot, 1955).

2.1.1. Constitutive equation

Two constitutive equations govern poroelastic response. The first describes the relations between stress, strain, and pore pressure:

$$\sigma = C\varepsilon - \alpha_B p_f I \quad (1)$$

where σ is the Cauchy stress tensor, ε is the strain tensor, C is the elasticity matrix, α_B is the Biot-Willis coefficient, p_f is the fluid pore pressure and I is the unit matrix.

A second constitutive equation relates the increment in fluid content ζ to volumetric strain and incremental pore pressure. The fluid pore pressure is proportional to the dilation of the porous matrix and the change of the fluid content:

$$p_f = M(\zeta - \alpha_B \varepsilon_{vol}) \quad (2)$$

where ε_{vol} is the volumetric strain, and Biot modulus M is the inverse of the storage coefficient S which can be defined through the following equation under constant volumetric strain:

$$S = \frac{1}{M} = \frac{\partial \zeta}{\partial p} \Big|_{\varepsilon_{vol}} \quad (3)$$

This definition allows the storage coefficient to be measured directly or calculated from basic material properties in the case of an ideal porous material.

2.1.2. Continuity equation

Darcy's law is required to describe fluid flow in the poroelastic material as

$$v = -\frac{k}{\mu} \nabla p \quad (4)$$

where v is the Darcy velocity, k is the permeability, μ is the viscosity and ∇p is the pore pressure gradient.

When Darcy's law is combined with the continuity equation

$$\frac{\partial \rho}{\partial t} + \nabla \cdot (\rho v) = 0 \quad (5)$$

where ρ is the fluid density, t is the time. Then it yields the governing

Table 1

Typical values for the properties of shale gas reservoirs (Roussel, 2011).

Permeability, k	1e-18 [m ²]
Viscosity, μ	2e-5 [Pa s]
Young's Modulus, E	3.45e10 [Pa]
Rock Density, ρ_s	2500 [kg/m ³]
Fluid Density, ρ_f	136.7 [kg/m ³]
Poisson's Ratio, ν	0.3
Biot Coefficient, α	0.7
Porosity, ϕ	0.05
Fluid Compressibility, c_f	2.9e-8 [1/Pa]
Initial reservoir pressure, p_{res}	28 [MPa]
Bottomhole Flowing Pressure, p_{wf}	7 [MPa]
Maximum Principal Stress, σ_{max}	31.7 [MPa]
Minimum Principal Stress, σ_{min}	31 [MPa]
Fracture Maximum Width, w	4 [mm]

equation for flow in poroelastic media as

$$\rho S \frac{\partial p_f}{\partial t} + \nabla \cdot (\rho v) = Q_m - \rho \alpha_B \frac{\partial \varepsilon_{vol}}{\partial t} \quad (6)$$

where Q_m is the source of mass.

2.1.3. Mass balance equation

Solid deformation can be represented through Navier's equations for a solid in equilibrium under gravitational load as

$$-\nabla \cdot \sigma = \rho_{av} g - \rho_{av} \frac{\partial^2 u}{\partial t^2} \quad (7)$$

$$\rho_{av} = (1 - \phi) \rho_s + \phi \rho_f \quad (8)$$

where ρ_{av} is the average density of fluid and solid matrix and g is the gravitational acceleration, u is the flow velocity and the second term on the right hand-side of Eq. (7) is the inertial term - set to zero, since in the laminar regime viscous forces dominate. ρ_s and ρ_f are the densities of the solid and the fluid phase, respectively, and ϕ is porosity of the porous medium.

3. Model implementation

The reservoir model accommodates the following assumptions: 1), temperature is assumed to be constant; 2), the wellbore flows at constant pressure p_{wf} ; 3), the reservoir produces with no-flow/no fluid influx boundaries at the exterior; 4), there is a single fluid which is gas; 5), the "hydraulic" fracture has infinite conductivity.

The model is implemented in 2-D on a rectangular cell (1 m×0.75 m) containing an elliptical fracture (a=0.12 m, b=2 mm) and a central wellbore (r=5 mm) (Fig. 2). The domain is scaled to minimize execution time with all properties reported in non-dimensional quantities. The analyses follow the statement of Roussel and Sharma (2010), who proposed that the boundaries have no impact on the dimensions of the stress reversal region if the distance from the fracture to the boundaries is at least three times the fracture half-length (Roussel and Sharma, 2010). COMSOL Multiphysics is used for this coupled model and meshing is auto-calibrated for fluid dynamics. The completed mesh consists of 3306 elements.

Berchenko and Detournay (Berchenko and Detournay, 1997) developed dimensionless parameters that minimize the number of independent parameters and simplify the type-curves calculation. These dimensionless parameters can be applied to any reservoir properties and fracture geometries. In order to investigate the time dependency of the size of stress reversal region, dimensionless time τ is used for time mapping and is defined as

$$\tau = \frac{4kt}{\mu L_f^2 \left(c_f \phi + \frac{\alpha_B (1+\nu)(1-2\nu)}{(1-\nu)E} \right)} \quad (9)$$

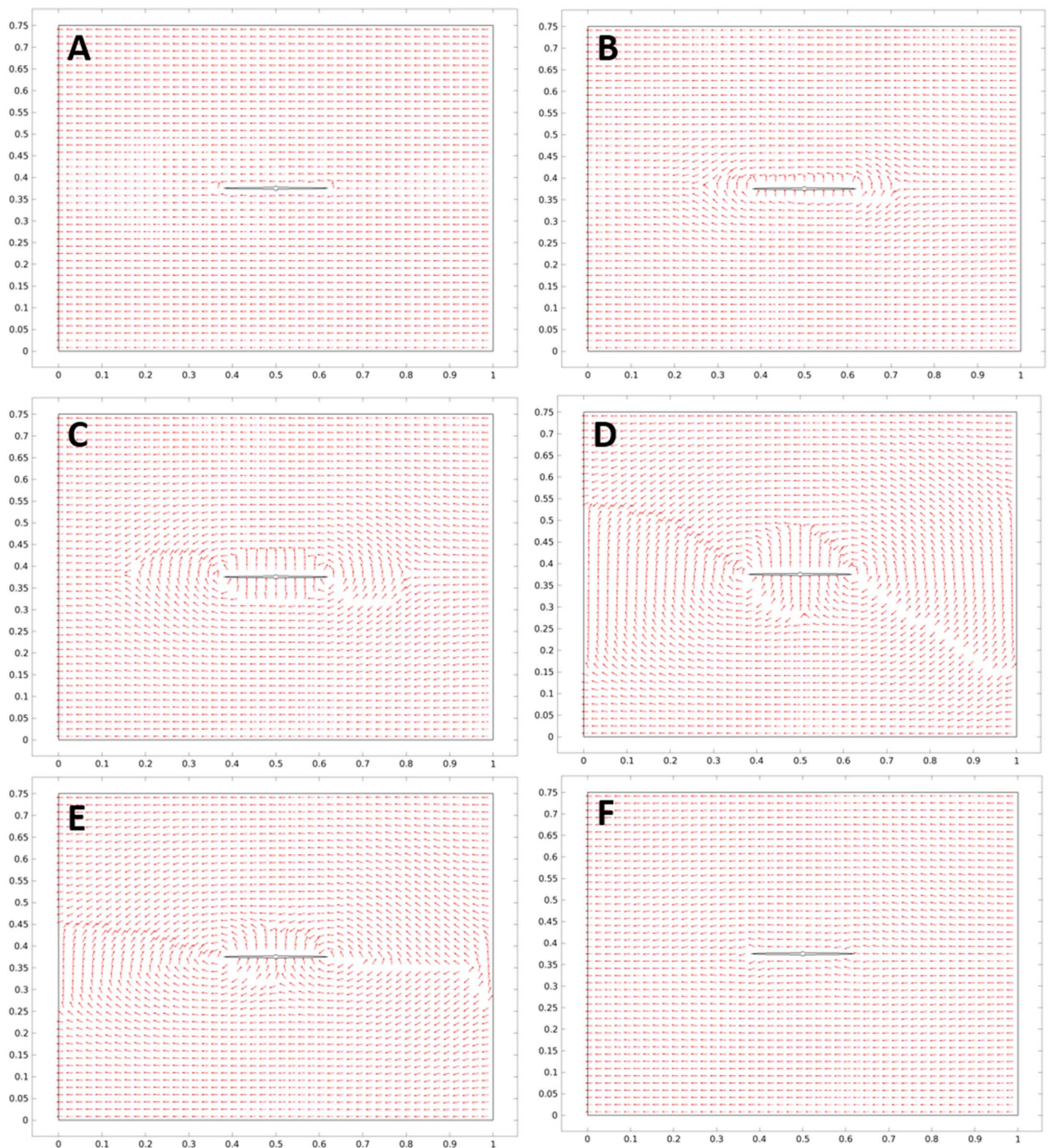


Fig. 3. Evolution of stress reversal region at A) $\tau=0$; B) $\tau=0.07$; C) $\tau=0.39$; D) $\tau=9.6$ (optimal timing); E) $\tau=47.5$; F) $\tau=100$.

where k is the average reservoir permeability [m^2], t is the production life [s], L_f is the fracture half-length [m], μ is the fluid viscosity [$Pa\cdot s$], c_f is the fluid compressibility [$1/Pa$], ϕ is the porosity, α_B is the Biot coefficient, ν is the Poisson’s ratio, E is the Young’s modulus [Pa].

Reservoir conditions used in the simulation for the base case are listed in Table 1. Displacement is permitted along the fracture faces where a constant stress is imposed. This stress is equal to the net pressure p_{net} (which is considered as zero in this model) plus the minimum principal stress σ_{min} . This uniform stress boundary condition

applied on the fracture face is the pressure required for the proppant to retain the fracture open. No flow boundaries with constant stress conditions (σ_{min} in y -direction and σ_{max} in x -direction) are applied normal to the “block” face (Fig. 2). Wellbore and fracture face flow at constant bottomhole flowing pressure p_{wf} .

4. Results and discussion

Parametric studies explore the time dependency of stress reorienta-

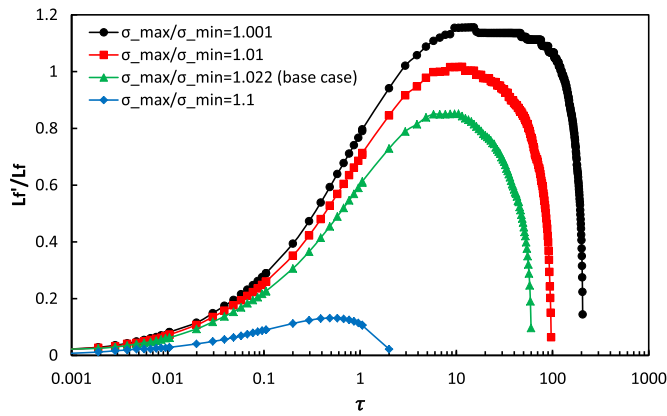


Fig. 4. L_f'/L_f vs. τ for different $\sigma_{h\ max}/\sigma_{h\ min}$ ratio.

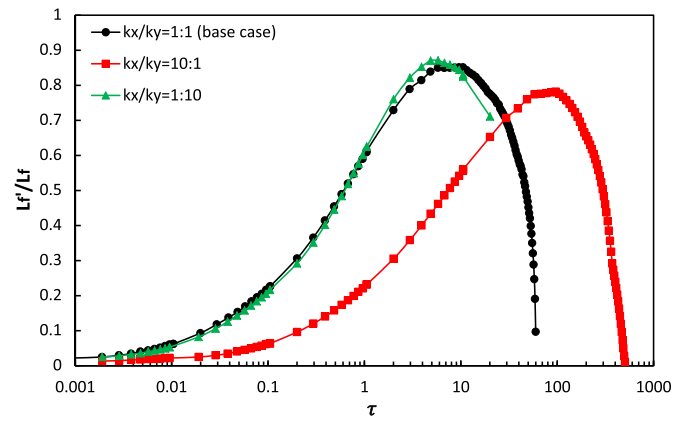


Fig. 7. L_f'/L_f vs. τ for permeability anisotropy.

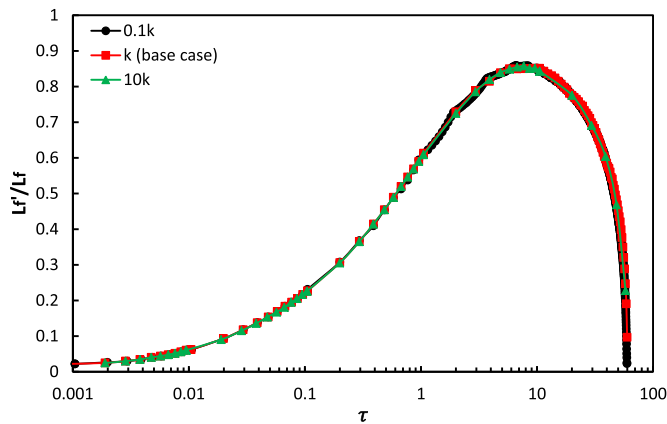


Fig. 5. L_f'/L_f vs. τ for different permeability.

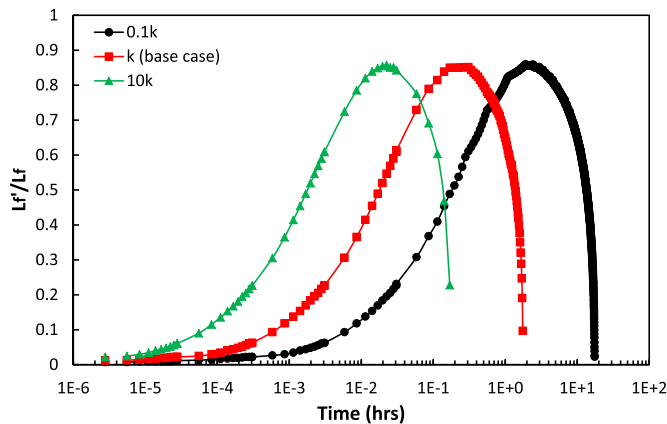


Fig. 6. L_f'/L_f vs. time for different permeability.

tion, threshold stress ratio $\sigma_{h\ max}/\sigma_{h\ min}$ for the presence of the stress reversal region (stress anisotropy), the influences of permeability anisotropy/heterogeneity, pressure drawdown and rock-fluid properties on the evolution of the stress reversal region. Dimensionless time τ and the ratio L_f'/L_f (Fig. 1) are used to quantify the size of the stress reversal region over the logarithm of time scale. The direction of the maximum principal stress with a deviation of more than 45° from the initial state is considered as the criterion for the occurrence of stress reorientation.

Fig. 3 shows the evolution of the distribution of the direction of the maximum principal stress with dimensionless time τ . The stress reversal region develops immediately as the reservoir begins to produce and reaches its maximum extent when the flow around the fracture transits from linear flow to radial flow – this is confirmed from the

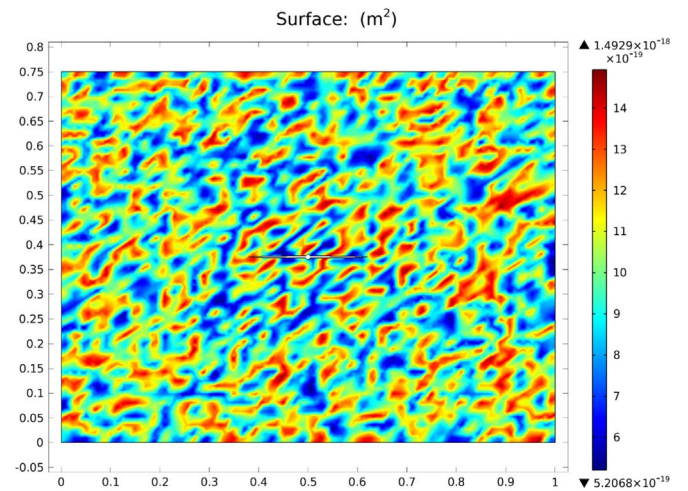


Fig. 8. Heterogeneous permeability distribution in the reservoir.

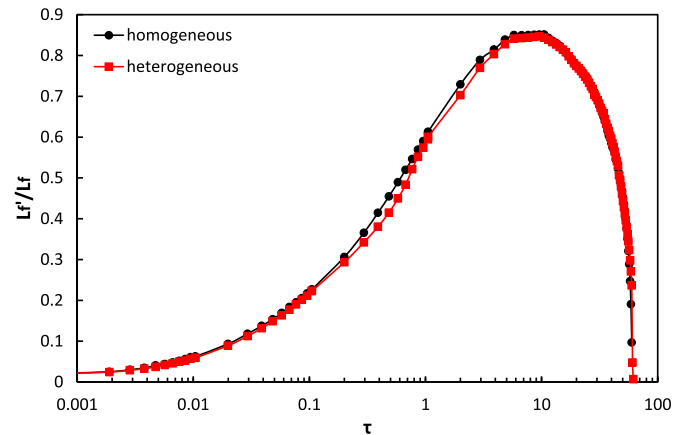


Fig. 9. L_f'/L_f vs. τ for permeability heterogeneity.

pressure surface profile (figures not shown). After reaching a maximum extent, the stress reversal region shrinks and the direction of the maximum principal stress gradually returns to its initial state (is parallel to the existing fracture). As apparent in Fig. 3D, $\tau=9.6$ is the optimal timing to refract in that L_f' , the proxy for the size of the stress reversal region, reaches a maximum dimension.

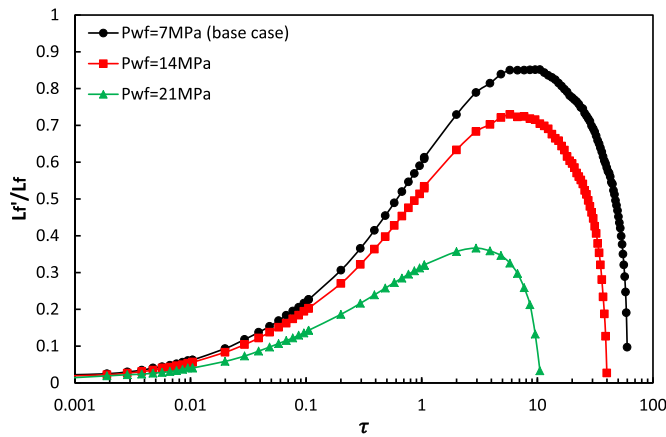


Fig. 10. L_f'/L_f vs. τ for different pressure drawdown.

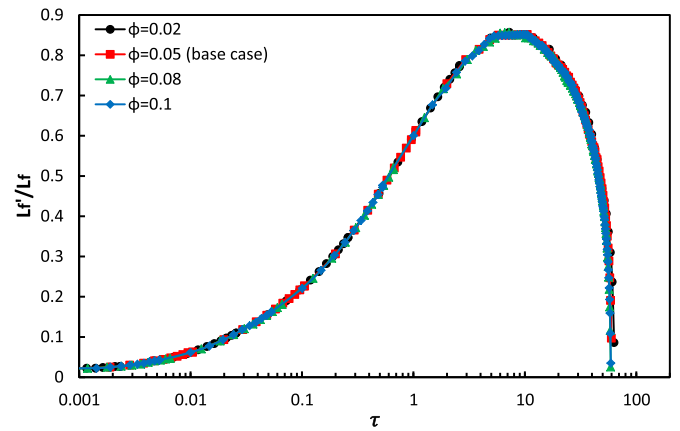


Fig. 13. L_f'/L_f vs. τ for different porosity.

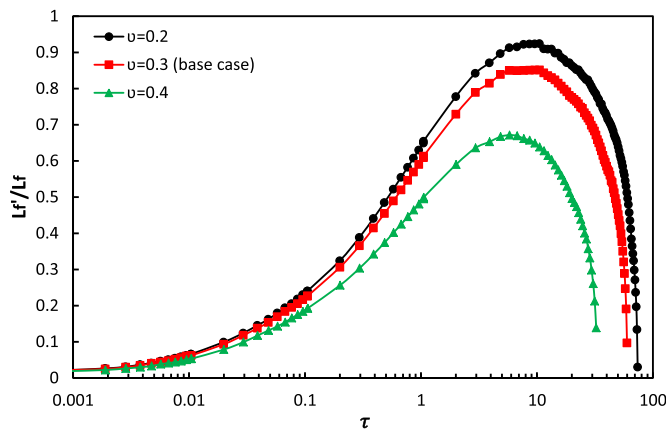


Fig. 11. L_f'/L_f vs. τ for different Poisson's ratio.

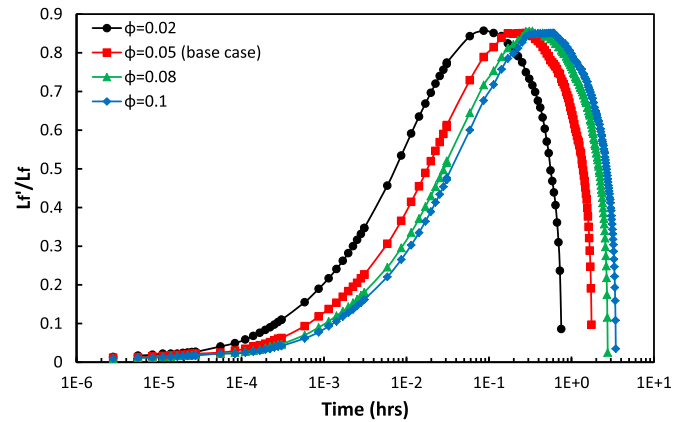


Fig. 14. L_f'/L_f vs. time for different porosity.

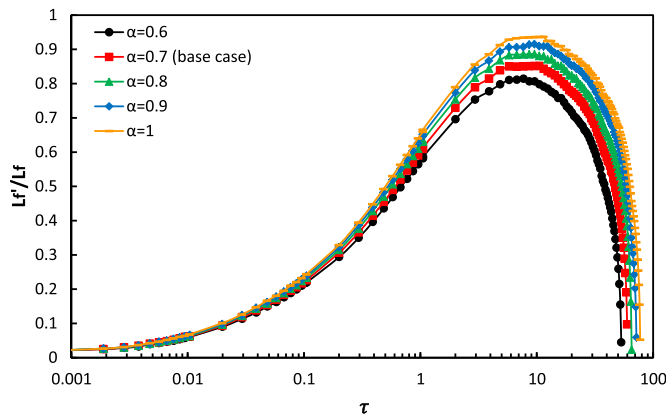


Fig. 12. L_f'/L_f vs. τ for different Biot coefficient.

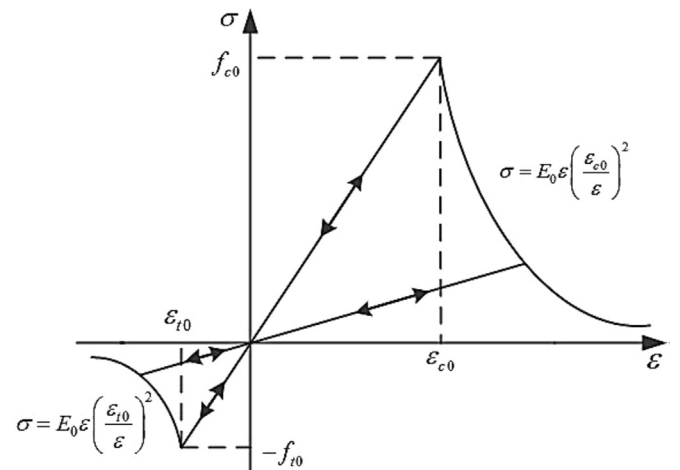


Fig. 15. The constitutive law of rock under conditions of uniaxial stress.

4.1. Effect of stress anisotropy

The stress reversal region concept relies on an initially small difference between the maximum and minimum horizontal stresses, which often holds true for tight gas reservoirs (Aghighi et al., 2009). The difference between minimum ($\sigma_{h \min}$) and maximum ($\sigma_{h \max}$) principal stress used for the base case in this study is 0.7 MPa ($\sigma_{h \max} / \sigma_{h \min} = 1.022$) (Table 1). Several $\sigma_{h \max} / \sigma_{h \min}$ ratios are tested in order to determine the threshold for the presence of stress reorientation (Fig. 4). Fig. 4 shows that this threshold value is ~ 1.1 . At this peak ratio a very small stress reversal region is quickly developed and then immediately vanishes. Apparent from Fig. 4, the closer the $\sigma_{h \max} / \sigma_{h \min}$ ratio approaches to 1, the more significant the stress reorienta-

tion. The optimal timing to refract is also postponed when this ratio becomes approaches 1. For the base case examined in this study, the optimal time to refract is when $\tau = 9.6$ where L_f'/L_f is 0.85.

4.2. Effect of permeability magnitude

For the base case the permeability k is chosen as $1e-18 \text{ m}^2$ (Table 1). Two other cases with permeability 0.1 and 10 times that of the base case are examined to investigate the effect of permeability magnitude. Figs. 5 and 6 show the length ratio L_f'/L_f with dimensionless time τ and production time t for these different permeabilities. Although permeability magnitude has no influence on the optimal

refrac timing on the dimensionless time scale (Fig. 5), because the effect is normalized by Eq. (9), there is significant difference on the true production time scale for different values of permeability (Fig. 6). The pressure gradient in the reservoir has to exceed a specific value in order to have a higher stress reduction in the direction parallel to the initial fracture to overcome the initial small stress difference. In reservoirs with higher permeability, the pressure gradient spreads out faster and so does the stress reversal region. Fig. 6 implies that a small permeability has an extended optimal refrac timing. The multiples between the optimal refrac timing of each case is the reciprocal of the multiples between the permeability of each case. However permeability magnitude has no effect on the size of resulting stress reversal region as all three cases show the same L_f^*/L_f value.

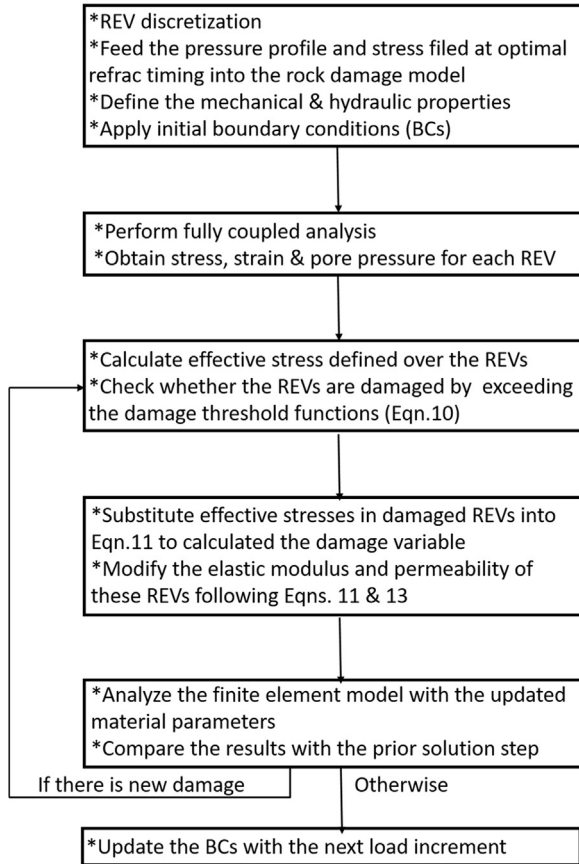


Fig. 16. Work flow of fracture propagation simulation using a rock damage model.

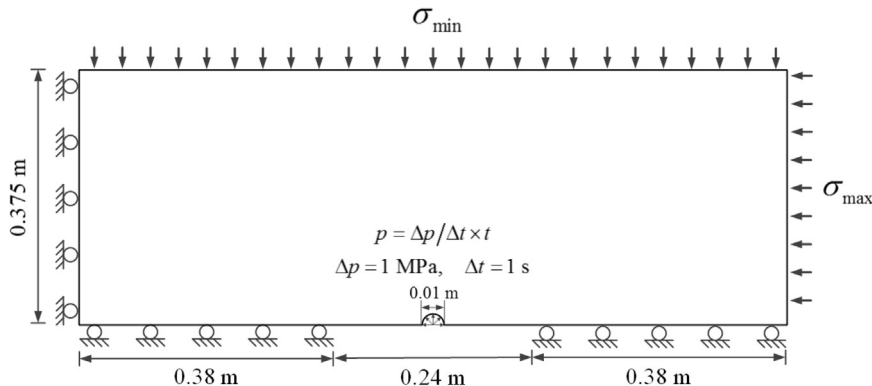


Fig. 17. Model set up for refracturing modeling.

Table 2
Parameters related to damage model.

Initial uniaxial compressive strength f_{c0}	115.0 MPa
Initial uniaxial tensile strength f_{t0}	11.5 MPa
Damage-permeability effect coefficient α_k	5.0

4.3. Effect of permeability anisotropy

The effect of permeability anisotropy is analyzed following the same procedure. Two cases are investigated and compared to the base case which has an isotropic permeability. The permeability is ten times greater in the x-direction for the first case and for the second case the permeability is ten times greater in the y-direction. The anisotropic permeability affects the shape of the evolving drainage area that is stretched in the direction of higher permeability (confirmed by the pressure surface profile and figures not shown). Fig. 7 indicates that a refrac treatment is most efficient if the reservoir permeability is greater in the direction perpendicular to the initial fracture ($k_x/k_y=1:10$) and vice versa least efficient for the opposite condition ($k_x/k_y=10:1$). Permeability anisotropy is positively correlated to the size and negatively correlated to the timing if the permeability is greater in the direction perpendicular the initial fracture, however it is negatively correlated to the size and positively correlated to the timing if the permeability is greater in the direction parallel to the initial fracture.

4.4. Effect of permeability heterogeneity

The true heterogeneity of reservoirs may also affect the success of resfracs, and is examined here. The reservoir is divided into a grid with 50×50 blocks. The geostatistical function in Matlab is used to assign a heterogeneous permeability for each grid block. The generated permeabilities vary between $5.05e-19 \text{ m}^2$ and $1.50e-18 \text{ m}^2$ with an average of $1e-18 \text{ m}^2$ and standard deviation of $2.9e-19 \text{ m}^2$. These data are imported into COMSOL Multiphysics and distributed to individual meshes based on the coordinates by an interpolation function (Fig. 8). Fig. 9 shows that this level of permeability heterogeneity has no influence on the size of resulting stress reversal region nor optimal refrac timing.

4.5. Effect of pressure drawdown

Sensitivity analysis is also conducted on the impact of the magnitude of pressure drawdown. Fig. 10 shows that a larger pressure drawdown provides favorable conditions for a successful refracturing as suggested by a high L_f^*/L_f value. To the contrary, a higher bottom-hole flowing pressure p_{wf} limits the stress reorientation to the immediate vicinity of the wellbore with an early optimal refrac timing.

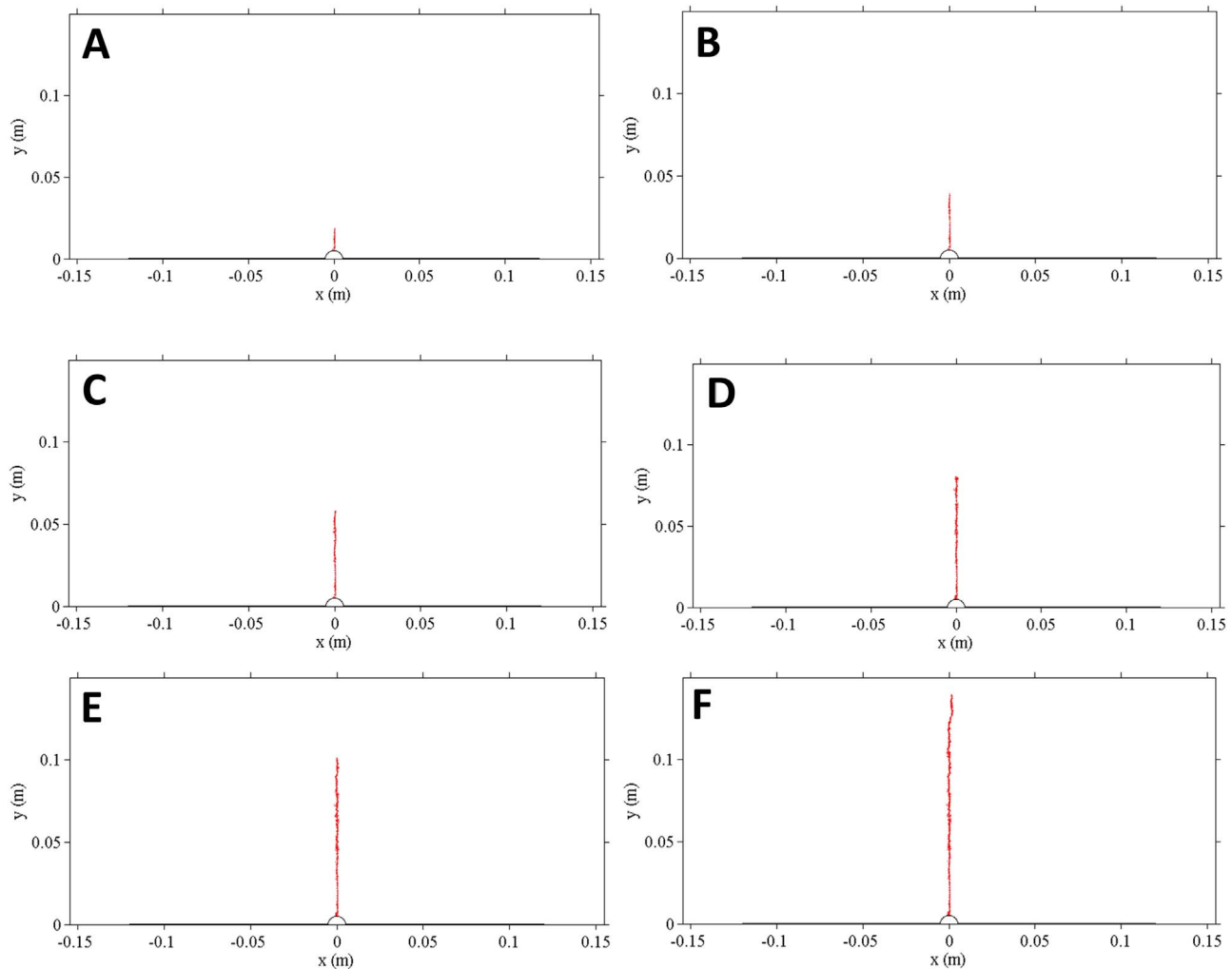


Fig. 18. Fracture propagation during the refracturing treatment under the effect of stress redistribution (Case 1). (A: $P_{inj}=45$ MPa; B: $P_{inj}=55$ MPa; C: $P_{inj}=65$ MPa; D: $P_{inj}=75$ MPa; E: $P_{inj}=85$ MPa; F: $P_{inj}=95$ MPa) (Figures are zoomed out for magnification.).

This is purely due to the production-induced stress reorientation which results from poroelasticity effect and also due to the choice of the parameter that defines the bounds of the stress reversal region.

4.6. Effect of Poisson's ratio

For a penny-shaped fracture where its height equals length, Poisson's ratio does not affect the resulting stress contrast since stresses are independent of Poisson's ratio (Sneddon, 1946). However in most cases where fracture height is smaller than fracture length, Poisson's ratio will play a part. Fig. 11 shows that a propped fracture creates a greater stress contrast in its vicinity with a low Poisson's ratio in that a low Poisson's ratio indicates that the deformation in the direction parallel to the fracture is small compared to the deformation normal to the fracture – from this a larger stress contrast develops.

4.7. Effect of Biot coefficient

Examining the sensitivity to variations in the Biot coefficient (Fig. 12) shows that there is a positive correlation between Biot coefficient and the size of the stress reversal region. A reservoir with a large Biot coefficient shows a slightly delayed optimal refrac timing. As Biot coefficient approaches zero, there should be no poroelastic effect and hence no consequent stress reversal with time.

4.8. Effect of porosity

Typical average values for the porosity of sedimentary rocks (Barrell, 1914) are of the order: shale, 0.082; sandstone, 0.148; limestone, 0.053; and all sedimentary rocks, 0.085. Additional data since the publication of Barrell's summary indicate that the average value of 0.082 for the porosity of shale may be low. Based on the data above, a range of porosity from 0.02 to 0.1 is examined to investigate the effect of porosity. Figs. 13 and 14 show the values of L_f'/L_f over dimensionless time τ and production time t under different porosities. Although porosity has no influence on the optimal refrac timing on the dimensionless time scale (Fig. 13), since its effect is normalized by Eq. (9), there is significant difference on the real production time scale for different values of porosity (Fig. 14). Fig. 14 implies that larger porosity contributes an extended optimal refrac timing. The multiples between the optimal refrac timing of each case is the reciprocal of the multiples between the porosity of each case. However porosity has no effect on the size of stress reversal region.

5. Fracture propagation under the effect of stress redistribution

A coupled model of rock damage and fluid flow is used to simulate the fracture propagation under the effect of stress redistribution during the refracturing treatment. The nonlinear stress-strain relation of rock under uniaxial tension and compression can be simplified as a

piecewise function (Fig. 15) (positive for compression). Tension or shear damage is initiated when the stress state of a representative elementary volume (REV) satisfies the maximum tensile stress criterion or the Mohr–Coulomb criterion respectively, which are shown as follow (Zhu and Tang, 2004):

$$\begin{cases} F_1 = -(\sigma_3 - ap) - f_{t0} = 0 \\ F_2 = (\sigma_1 - ap) - \frac{1 + \sin\theta}{1 - \sin\theta}(\sigma_3 - ap) - f_{c0} = 0 \end{cases} \quad (10)$$

where F_1 and F_2 are two damage threshold functions; σ_1 and σ_3 are the maximum and minimum principal stress, respectively; f_{t0} and f_{c0} are the uniaxial tensile and compressive strength, respectively; θ is the internal friction angle, p is the pore pressure and a is the Biot coefficient.

The elasticity modulus of a REV may be considered to decrease monotonically with the evolution of damage as

$$E = (1 - D)E_0 \quad (11)$$

where E_0 and E are the elasticity modulus of an REV before and after the initiation of damage, respectively; D is the damage variable that varies from 0 to 1. Based on the constitutive law shown in Fig. 15, the damage variable can be defined as

$$D = \begin{cases} 0 & F_1 < 0 \quad \text{and} \quad F_2 < 0 \\ 1 - \left(\frac{\varepsilon_{t0}}{\varepsilon_3}\right)^2 & F_1 = 0 \quad \text{and} \quad dF_1 > 0 \\ 1 - \left(\frac{\varepsilon_{c0}}{\varepsilon_1}\right)^2 & F_2 = 0 \quad \text{and} \quad dF_2 > 0 \end{cases} \quad (12)$$

where ε_{t0} and ε_{c0} are maximum tensile and compressive principal strain, respectively. In the numerical implementation of Eq. (11), the potential for tensile damage is examined first with the maximum tensile stress criterion, and only the REV's that are not damaged in tension will be examined for subsequent damage in shear with the Mohr–Coulomb criterion.

After damage initiates, the elastic modulus changes (Eq. (11)) and impacts permeability as damage evolves. The permeability evolution with damage is a complex process and here we describe this relation as the exponential function

$$k = k_0 \exp(\alpha_k D) \quad (13)$$

where k_0 is the initial permeability and α_k is a constant selected here as equal to 5 and defined as the damage-permeability coefficient to indicate the effect of damage on the permeability.

A coupled model of rock damage and fluid flow results from combining Eqs. (1)–(7), (10)–(12) where the Young's modulus and permeability are functions of the damage. The complete set of coupled

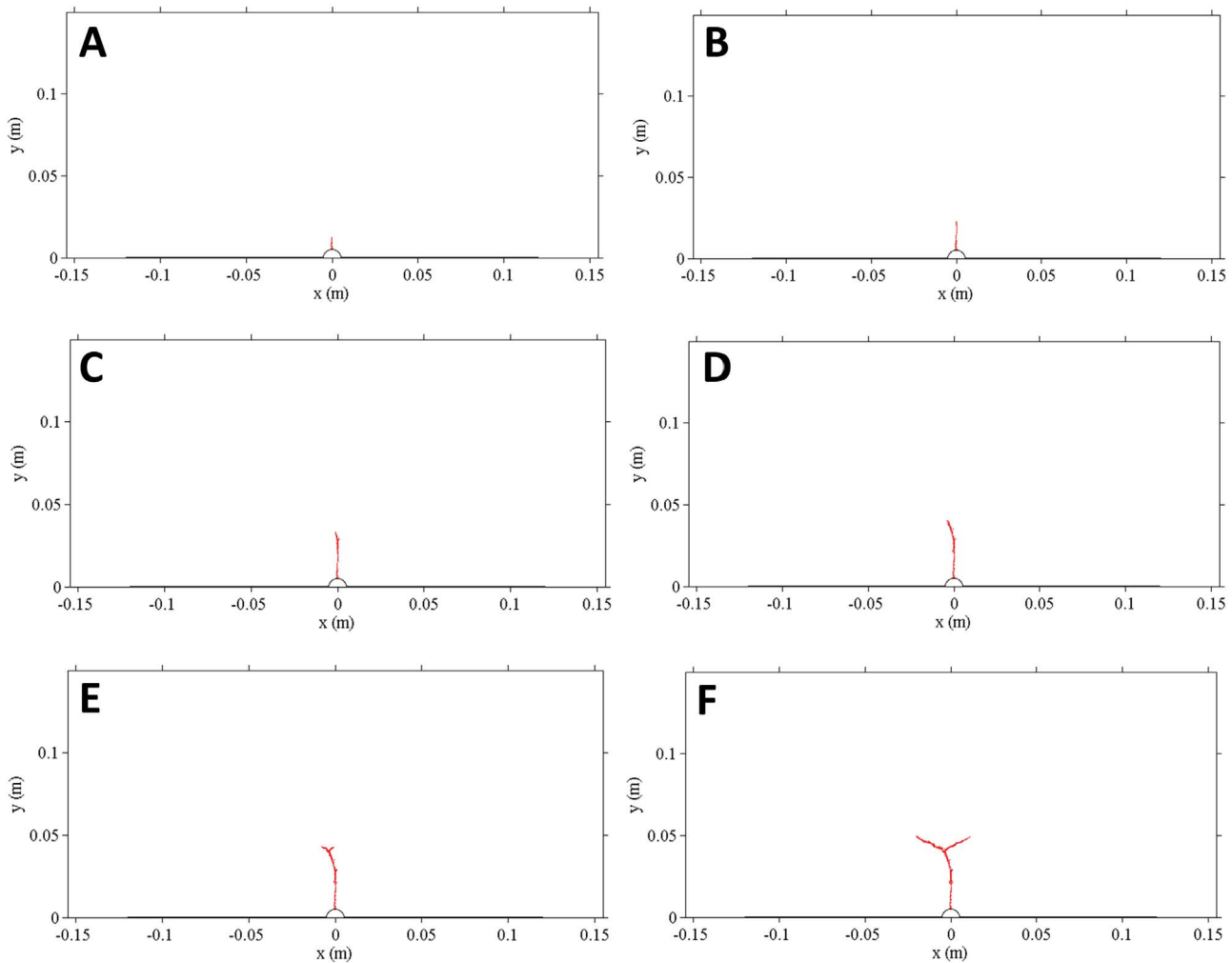


Fig. 19. Fracture propagation during the refracturing treatment under the effect of stress redistribution (Case 2). (A: $P_{inj}=31$ MPa; B: $P_{inj}=36$ MPa; C: $P_{inj}=41$ MPa; D: $P_{inj}=45$ MPa; E: $P_{inj}=47$ MPa; F: $P_{inj}=56$ MPa) (Figures are zoomed out for magnification.).

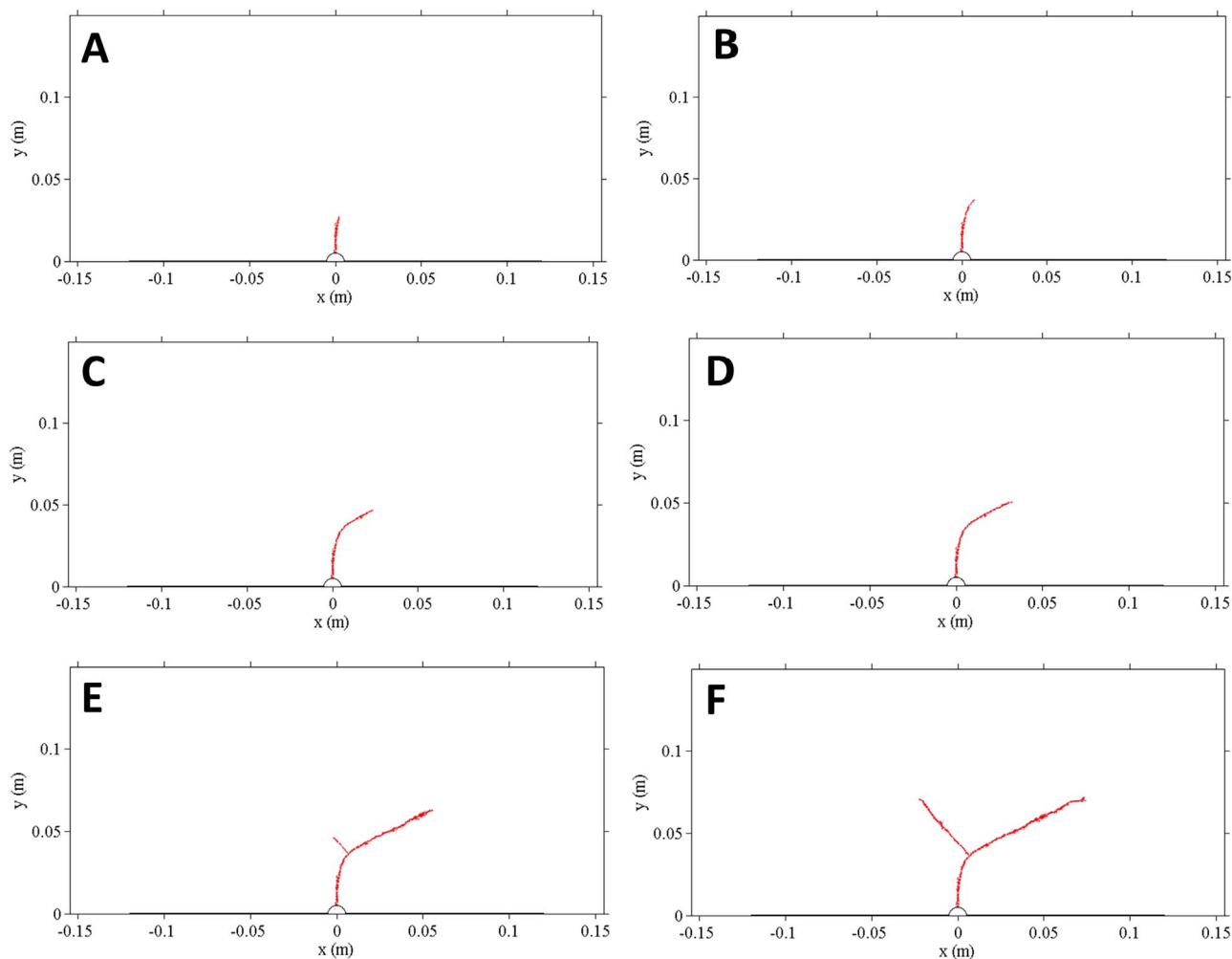


Fig. 20. Fracture propagation during the refracturing treatment under the effect of stress redistribution (Case 3). (A: $P_{inj}=51$ MPa; B: $P_{inj}=54$ MPa; C: $P_{inj}=59$ MPa; D: $P_{inj}=62$ MPa; E: $P_{inj}=69$ MPa; F: $P_{inj}=80$ MPa) (Figures are zoomed out for magnification.).

Table 3
Summary of the effects of different factors.

	Stress reversal region size	Optimal refrac timing
$\sigma_h \max / \sigma_h \min$	(-)	(-)
Permeability Magnitude	N/A	(-)
Permeability Anisotropy	(+)/(-)	(-)/(+)
Permeability Heterogeneity	N/A	N/A
Pressure Drawdown	(+)	(+)
Poisson's Ratio	(-)	(-)
Biot Coefficient	(+)	(+)
Porosity	N/A	(+)

(+) means positive correlation; (-) means negative correlation; N/A means no effect.

equations is solved by the finite element method. The damage variable and changes in the damage-induced elastic modulus and permeability are calculated and updated as the loads increase. The workflow is summarized as follows (Fig. 16) (Wang et al., 2015):

The above workflow is implemented in the code COMSOL Multiphysics with MATLAB scripting. Taking advantage of the half symmetry, the problem geometry is a rectangular region containing a half borehole located along the base as shown in Fig. 17. The initial values of stress and pore pressure of this study are identical to those in the stress reversal simulation when the stress reversal effect is optimal and the dimensionless time, τ , is equal to 9.6. The boundary conditions are shown in Fig. 17. This problem can be analyzed by assuming plane strain conditions and transient fluid flow. A roller is applied on the left

and basal boundaries to represent the symmetry. Far field stresses σ_{min} and σ_{max} are applied on the top and right boundaries. All boundaries are zero flux except for the borehole where the fluid is injected as an increasing hydraulic pressure p with time. The geometry is divided into a grid of 5000×1875 REVs. Initial hydraulic pressure in the borehole is 26 MPa and the pressurization rate is 1 MPa/s. The problem domain is discretized into 51,492 triangle elements with a refined size around the borehole where the fracture is expected to be formed. The values for properties of reservoir and fracturing fluid are shown in Table 1. The parameters related to the damage model are listed in Table 2.

Several cases are investigated and the results are shown in Figs. 18 and 19. In the first case (Fig. 18), the stress applied on the initial fracture face is the same as the minimum principal stress and the ratio between the maximum and minimum principal stress in the reservoir is 1.022, which is the value used for the prior base case. Results show that during the refracturing treatment, the second fracture grows perpendicular to the initial fracture, confirming the existence of the stress redistribution. However due to the mechanical effect resulting from the stress applied on the initial fracture face, no isotropic point is observed.

In the second case (Fig. 19), the stress applied on the initial fracture face is $0.7 \times$ minimum principal stress and the ratio between the maximum and minimal principal stress in the reservoir is also 1.022. Results show that the second fracture initiates and propagates normal to the initial fracture. An isotropic point is also observed where the fracture turns paralleled to the initial hydrofracture beyond this isotropic point.

In the third case (Fig. 20), the stress applied on the initial fracture face is the same as minimum principal stress and the ratio between the maximum and minimum principal stress in the reservoir is 1.1, which is the threshold to have a stress reversal region. Results show that the second fracture initiates and propagates normal to the initial fracture. An isotropic point is also observed and the fracture turns parallel to the initial massive hydrofracture (initial treatment) beyond this isotropic point.

6. Conclusion

This study examines the optimal refrac timing and the dimensions of the stress reversal region under different reservoir conditions using a coupled poroelastic-mechanical model. Key factors including the time dependency of the stress reorientation, threshold of the stress ratio $\sigma_{h\ max}/\sigma_{h\ min}$ for the presence of the stress reversal region, the influences of permeability anisotropy/heterogeneity, pressure draw-down and rock-fluid properties control the evolution of the stress reversal zone. Results, summarized in Table 3, show that the size of the stress reversal region and optimal refrac timing are positively or negatively correlated to the parameters examined in the study.

Fracture propagation during the refracturing treatment is examined using a coupled model of rock damage and fluid flow. Results show that the second fracture initiates and propagates perpendicular to the initial fracture and indeed turns parallel to the initial hydrofrac beyond the isotropic point, confirming the existence of a stress reversal region.

References

- Aghighi, M.A., Rahman, S.S., Rahman, M.M., 2009. Effect of formation stress distribution on hydraulic fracture reorientation in tight gas sands. SPE 122723.
- Barrell, J., 1914. The strength of the Earth's crust. *J. Geol.* 22, 214.
- Berchenko, I., Detournay, E., 1997. Deviation of hydraulic fractures through poroelastic stress changes induced by fluid injection and pumping. *Int. J. Rock. Mech. Min. Sci.* 34 (6), 1009–1019.
- Biot, M.A., 1955. Theory of elasticity and consolidation for a porous anisotropic solid. *J. Appl. Phys.* 26 (2), 182–185.
- Chen, H.-Y., Lawrence, W., 2001. Reservoir Stress Changes Induced by Production/Injection. SPE Rocky Mountain Petroleum Technology, Keystone, Colorado.
- Elbel, J.L., Mack, M.G., 1993. Refracturing: observations and theories. SPE Production Operations Symposium, Oklahoma City.
- Hagemann, B., Wegner, J., Ganzer, L., 2012. Investigation of hydraulic fracture re-orientation-re-orientation effect in tight gas reservoirs. COMSOL Conference, Milan.
- Liu, H., et al. 2008. Evaluation of refracture reorientation in both laboratory and field scales. SPE International Symposium and Exhibition on Formation Damage Control, Lafayette, Louisiana, USA.
- Mack, M.G., Elbel, J.L., 1994. Hydraulic fracturing orientation and pressure response During fracturing of producing wells. *Rock. Mech.*, 175–183.
- Roussel, N.P., 2011. Stress Reorientation in Low Permeability Reservoirs (Ph.D. Dissertation). The University of Texas, Austin, 30.
- Roussel, N.P., Sharma, M.M., 2010. Role of stress reorientation in the success of refracture treatments in tight gas sands. SPE 124491.
- Sayers, C.M., 2004. Monitoring production-induced stress changes using seismic waves. In: Proceedings of the SEG International Exposition and 74th Annual Meeting, Denver, Colorado.
- Siebrits, E., Elbel, J.L., 1998. Parameters affecting azimuth and length of a secondary fracture during a refracture treatment. SPE 48928.
- Siebrits, E., et al. 2000. Refracturing reorientation enhances gas production in barnett shale tight gas wells. SPE Annual Technical Conference and Exhibition, Dallas.
- Singh, V., Roussel, N.P., Sharma, M.M., 2008. Stress reorientation around horizontal wells. SPE 116092.
- Sneddon, I.N., 1946. The distribution of stress in the neighborhood of a crack in an elastic solid. *Proc. R. Soc. Lond.* 187, 229–260.
- Wang, J.H., et al. 2015. The influence of fracturing fluids on fracturing processes: a comparison between gas and water. In: Proceedings of the 49th US Rock Mechanics/Geomechanics Symposium, San Francisco.
- Weng, X., Siebrits, E., 2007. Effect of production induced stress field on refracture propagation and pressure response. SPE 106043.
- Wolhart, S., 2001. Hydraulic fracturing. s.l. SPE Distinguished Lecturer Series.
- Wolhart, S., Zoll, M., McIntosh, G., Weijers, L., 2007. Surface tiltmeter mapping shows hydraulic fracture reorientation in the codell formation, Wattenberg Field, Colorado. SPE Annual Technical Conference and Exhibition, Anaheim, California, U.S.A.
- Zhai, Z., Sharma, M.M., 2007. Estimating fracture reorientation due to long term fluid injection/production. SPE 106387.
- Zhou, L., Yang, G., Hou, Z., Were, P., 2015. Numerical modeling and investigation of fracture propagation with arbitrary orientation through fluid injection in tight gas reservoirs with combined XFEM and FVM. *Environ. Earth Sci.*, 73(THEMATIC), 5801–5813.
- Zhu, W.C., Tang, C.A., 2004. Micromechanical model for simulating the fracture process of rock. *Rock. Mech. Rock. Eng.* 37, 25–56.